Proceedings of ASME Turbo Expo 2011
GT2011
June 6-10, 2011, Vancouver, British Columbia, Canada

GT2011-45004

SOUND DEADENING ON FANS

Sascha Karstadt
Chair of Fluid Systems Technology
Technische Universität Darmstadt
Darmstadt, Germany
Email: Karstadt@fst.tu-darmstadt.de

Berthold Matyschok
Chair of Fluid Systems Technology
Technische Universität Darmstadt
Darmstadt, Germany
Email: Matyschok@fst.tu-darmstadt.de

Peter F. Pelz*
Chair of Fluid Systems Technology
Technische Universität Darmstadt
Darmstadt, Germany
Email: Pelz@fst.tu-darmstadt.de

ABSTRACT

In addition to the objective of increasing the efficiency of fans, acoustic efficiency gains more and more importance in order to reduce fan noise exposure. Whereas previously, research in this field was focused basically on blade design, nowadays the peripheral devices of fans are more often the object of study, since technical understanding of noise development is comparatively incomplete. Therefore, fundamental studies are essential to gain insight in the patterns of noise development and relatively easy opportunities to reduce noise level. In order to combine good aerodynamic properties with a silent fan, this experimental research investigates the acoustic and aerodynamic characteristics of an axial turbomachine and possibilities of reducing the emitted sound. Therefore a sound absorber ring is built directly around the rotor of a fan in order to absorb the sound very close to the origin. The fan assembly is installed in a test rig according to ISO 5136, which defines a standard for determining sound power radiated into a duct by fans. Acoustic signals are recorded with two microphones in the test duct, one on the pressure side, the second on the suction side, each close to anechoic terminations at the ends. The aerodynamic characteristics are determined with a calibrated inlet nozzle and static pressure measurements over the fan stage. To confirm the expectation that a significant part of the emitted sound power is tip clearance noise, which changes with the operating point, the volume flow of the fan is varied over its entire operating range. In this study, five different porous materials are tested for their ability of deadening the sound of the fan. In order to measure the influence of the construction which contains the materials, the perforated casing ring with a sound-reflecting termination and a plane ring with the same tip clearance are measured additionally as a reference. The noise exposure is analyzed over the complete frequency spectrum in order to determine the absorbing frequencies of the materials.

INTRODUCTION

Fans have a very large range of application, from small fans for cooling CPUs to big fans for example in wind tunnels. Nature and size vary significantly depending on their application. With increasing disturbances of daily life by different noise sources, especially in the vicinity of people, the interest in reducing noise emission grows. Possibilities are, on the one hand, a direct influence on sound development, e.g. by constructive changes of the rotor geometry or by reducing the rotational speed of the fan. On the other hand, passive or active measures of secondary sound reduction can be applied.

In this experimental study, the effectiveness of a sound absorber with porous materials installed in the casing region around the rotor of a fan is analyzed. Seven different configurations consisting of five sound absorber materials installed in a perforated casing ring are tested. To determine the influence of the perforated casing ring, two reference measurements are performed. Studies in an impedance tube show the absorbing coefficients of the used materials and their frequency dependence. The fan and the sound absorber configuration are installed in a test rig according to ISO 5136 [1], which defines a standard for determining of sound power radiated into a duct by fans.

It has been shown, inter alia in [2] that a significant part of the

*Address all correspondence to this author.

NOMENCLATURE

A	Area
A_D	Duct cross sectional area
A_R	Ring cross sectional area
D	Inner duct diameter
D_i	Hub diameter
D_o	Outer fan diameter
K	Calibration coefficient
L_p	Sound pressure level
L_w	Sound power level
$L_{w,spez}$	Specific sound power level
M	Torque
$\dot{V}$	Volume flow rate
Re	Reynolds number
S	Tip clearance
c	Speed of sound
c_a	Velocity of propagation
f	Frequency
n	Rotational speed
p_d	Dynamic pressure
p_s	Static pressure
p_t	Total pressure
s	Relative tip clearance
Greek symbols	
Δp_D	Static pressure difference
Δp_t	Total pressure difference
Δp_K	Static pressure difference
α	Absorption coefficient
η	Efficiency with total pressure rise
ν	Hub-tip ratio
ρ	Air density
σ	Porosity
φ	Flow coefficient
χ	Structure coefficient
ψ	Pressure coefficient

emitted sound power is caused by the tip leakage flow whose strength varies, depending on the operating point. Due to the pressure difference between suction and pressure side of the rotor blade, a tip leakage flow through the tip clearance between the rotating blades and the stationary casing is generated. Additionally, the flow through the tip clearance is deflected by the mainstream into the direction of the trailing edge. The flow rolls up to a spiral vortex on the suction side of the blade and induces a drag. Size and circulation of this vortex, according to Helmholtz's vortex theorem, depend on the bound vortex and the size of the tip clearance. In the limit $s = S/D_o \rightarrow 0$, no tip leakage vortex is formed. According to Helmholtz's vortex theorem the leading edge vortex in this case would reach infinite radius. In the limit $S/D_o \rightarrow \infty$ (no casing), the tip leakage vortex is of the same strength as the leading edge vortex. Depending on the operating point, the trajectory of the tip leakage vortex can hit the pressure side of the adjacent blade which causes a disturbance of the flow around the blade. In addition to the aerodynamic losses, the vortex has an influence on the noise generation of the fan. Fukano and Jang [3] found that due to the tip leakage vortex, a region with very small flow velocities is formed, whose size grows with decreasing volume flow. Local reverse flows appear. High velocity fluctuations cause a broadband noise, in the interaction zone of the tip leakage vortex and the mainstream, as well as in the vortex core. With increasing tip clearance or reduced volume flow rate, the intensity and expansion of the velocity fluctuations result in an increase of the broadband noise. At the same time, the trajectory of tip leakage vortex moves towards the pressure side of the adjacent blade and the velocity fluctuations cause pressure fluctuations which lead to dipole type noise generation. Emmrich et al. [4] analyzed the influence of a casing treatment, consisting of 152 grooves, on a single stage compressor. The stable operating range and the total pressure rise could be increased, but with a decrease of efficiency. A positive influence of this casing treatment on the angle of incidence in the blade tip section along with a reduced blade load and tendency of flow separations was found, which causes a higher blade load in the remaining blade sections. Emmrich et al. also found a stabilization of the flow and a reduction in size of the region with very small flow velocities near the casing wall. Analysis of averaged total pressure distributions showed low total pressure regions with a strong periodical character, which are caused by a leakage and a re-entrance jet through the grooves. The frequency could be traced back to the product of the blade passing frequency (BPF) and the number of grooves in the blade passage.
The mode of action of self-recirculating casing treatments was studied by Hathaway [5]. He showed, with numerical simulations on a fan rotor, that both the bleed of low-energy fluid out of the casing region near the rotor and the injection of high-energy fluid in front of the stage can reduce the blockage area with very small flow velocities. The reason for the blockage region is the low-energy fluid in the casing regions and the tip leakage vortex. Self-recirculating casing treatments, consisting of a bleed and an injector port, have a positive impact on the total pressure rise and the efficiency of the fan rotor. Hathaway showed that this is caused by a reduction of the blockage region, which allows the blade tip section to increase the participation in the pressure rise of the blade.

EXPERIMENTAL SETUP AND METHODOLOGY

The experiments were performed on a fan test rig according to ISO 5136 [1] located at the laboratory of the Chair of Fluid Systems Technology at Technische Universität Darmstadt. This standard defines the required setup to measure and compare the emitted acoustic power of fans and other turbomachines. In this test case, a fan with nine skewed blades, 13 guide vanes, an outer diameter of $D_o = 0.63$ m and a hub-tip ratio of $\nu = 0.45$ was mounted to the test rig. The blades have a backward sweep in the hub and a forward sweep in the tip region. They were designed

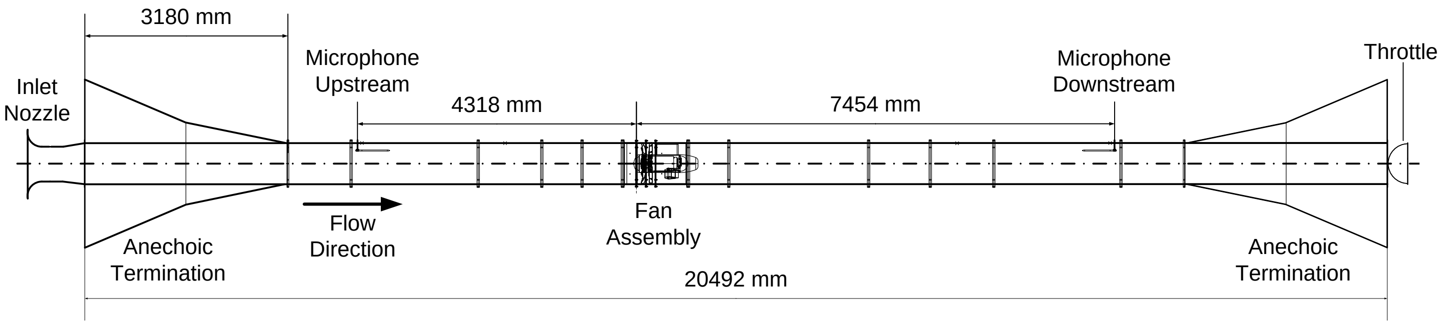

FIGURE 1. SKETCH OF THE TEST RIG

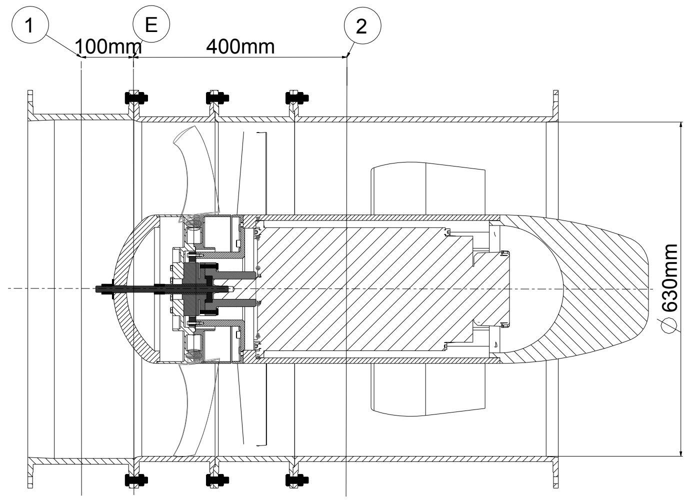

FIGURE 2. FAN ASSEMBLY

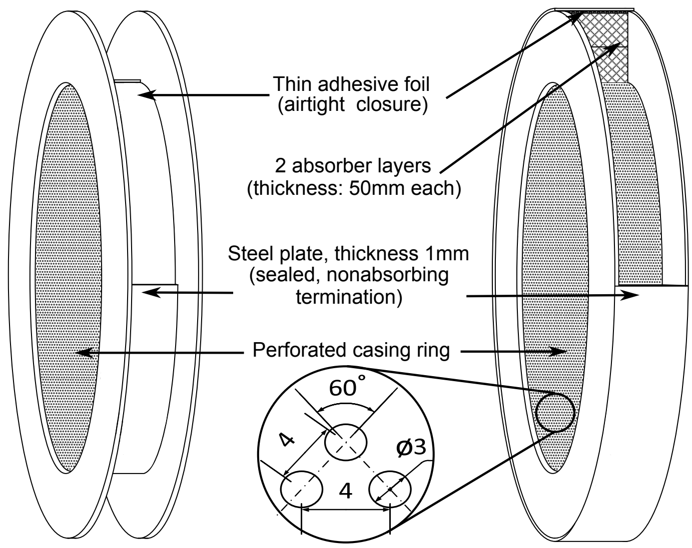

FIGURE 3. ABSORBER SETUP

for an operating point of $\varphi = 0.17$. As shown in Fig. 2, the fan assembly is partitioned into rings with different inner diameters which can easily be replaced to vary the tip clearance. The inner diameter of the flow path segments upstream and downstream of the rotor is designed in a way that even with the ring used for the largest tip clearance, there is always a reduction in the cross sectional area. This always leads to an accelerated flow while rounded edges at the occurring steps additionally avoid flow separation. For this study, a ring with a perforated surface with a thickness of 1 mm as shown in Fig. 3 is mounted in the test rig instead of the plain ring. The perforated structure with an axial length of 125 mm leads to a porosity $\sigma = \frac{A_{\text{hole}}}{A_{\text{total}}} \approx 0.6$. The resulting relative tip clearance is $s = S/D_{\text{o}} = 0.38\%$. To study the aerodynamic and acoustic characteristics of the perforated structure, two reference cases are measured. On the left side of Fig. 3, reference configuration 1 is shown. The backside of the perforated surface is sealed with an airtight thin adhesive foil and a sound-reflecting steel plate. In reference configuration 2, the same configuration is used but the perforation is sealed with paraffin to ensure a plain surface. The configuration with absorber materials is shown on the right side. Two absorber layers with a thickness of 50 mm each are closed airtight with a thin adhesive foil and sealed with a sound-reflecting steel plate. Five different commercially available absorber materials with different densities (Tab. 1) and a very broad variance in their characteristics are used for this study. F800FR is a nonwoven polyethersulfone, HR 290/71 is a soft foam on a melamine resin basis, 521 is a polyurethane ester acoustic foam, while R290 is a recycling product on melamine resin basis and R616 is a very dense recycling material. The surfaces of all studied materials are permeable to air and, except for HR290/71 and 521, top and bottom sides are equal. These two materials have a structured surface on one side.
During the experiments, the rotational speed is $n = 41.66\ \text{sec}^{-1}$

TABLE 1. ABSORBER MATERIALS

Material	1	2	3	4	5
Name	F800FR	HR290/71	521	R290	R616
ρ in kg/m^3	28.2	8.5	27.2	43.6	195.7

to achieve a constant Reynolds number of $Re = \pi n D_o^2/\nu = 3.5 \cdot 10^6$ with kinematic viscosity $\nu = 15 \cdot 10^{-6}$ m^2/s for air at standard conditions. A throttle at the pressure side end of the test rig is used to vary the volume flow rate $\dot{V}$ by changing counter pressure.

Volume Flow Rate

Measurements of the volume flow rate are performed with a calibrated inlet nozzle. The static pressure difference between the ambient and the accelerated flow inside the nozzle with a calibration coefficient K is used to calculate the air speed in a given area. In case of the used inlet nozzle K is constant and the volume flow rate can be calculated as $\dot{V} = K\sqrt{\Delta p_D/\rho}$. The six pressure measuring locations distributed over the circumference of the inlet nozzle are connected by a circular manifold, to connect and average the pressure.

Pressure

Pressure measurements are performed with a 16 channel scanner by Pressure Systems. Calibration allows the 16 channels to be measured simultaneously with an absolute uncertainty of less than 1 Pa. The total pressure rise of the fan is determined by two static pressure measurements. Figure 2 shows two measuring planes - 1 and 2. In each plane, six static pressure drills are distributed over the circumference. Knowing the volume flow rate and the static pressure difference over the fan stage $\Delta p_K = p_2 - p_1$, the total pressure rise can be calculated as

$$\Delta p_t = p_{t_2} - p_{t_1} = \Delta p_K + \frac{\rho}{2}\left(\frac{\dot{V}}{A_R}\right)^2 \left[1 - \left(\frac{A_R}{A_D}\right)^2\right]. \quad (1)$$

The dynamic pressure is determined by the volume flow rate. A_D denotes the circular cross sectional area of the duct. A_R describes the ring cross sectional area at plane 2. Due to the guide vanes behind the rotor, there is only negligible swirl at plane 2. The same is true for plane 1.

Torque

To determine the aerodynamic efficiencies of the fan, an input power has to be obtained. A flying mounted torque flange manufactured by Manner Sensortelemetrie was installed between the driveshaft and the fan, to measure the torque. Due to the direct installation at the rotor, the torque M is measured without any bearing friction torque. Because of the small surface, disc friction torque is negligible compared to the aerodynamic torque.

Dimensionless Products

In order to allow comparisons with other turbomachines, the characteristic curves are always plotted with dimensionless products. The dimensionless flow rate is the flow coefficient

$$\varphi = \frac{4\dot{V}}{n\pi^2 D_o^3}. \quad (2)$$

The dimensionless total pressure rise is given in form of the pressure coefficient

$$\psi = \frac{2\Delta p_t}{\rho\,(n\pi D_o)^2}. \quad (3)$$

With measured torque M and the rotational shaft speed n, the efficiency of the fan can be determined by:

$$\eta = \frac{\dot{V}\Delta p_t}{2M\pi n}. \quad (4)$$

Uncertainty of Measurement

The uncertainty of measurement of $\dot{V}$ is 1-1.3 % based on the actual volume flow. For η the uncertainty is below than 1.2 % absolute efficiency, according to actual pressure rise, volume flow rate and torque.

Sound

The sound within the duct is measured with two microphones each close to the anechoic terminations at the ends of the duct. The microphones are installed approximately seven times the inner duct diameter D upstream, and approximately eleven times D downstream of the reference plane E (Fig. 1). The pressure field microphones are manufactured by Bruel & Kjaer, with a recordable frequency range between 3.15 Hz and 20 kHz. In this study, the analyzed frequency range extends from 16 Hz to 16 kHz. Every item in the duct which is exposed to the turbulent flow generates a noise. To this purpose, microphones are installed in a turbulence screen to generate a minimal and known background noise at known frequencies, depending on the flow rate, which can be eliminated in later calculations. Using a two-channel microphone amplifier, the acoustic signals are recorded and analyzed with a computer. The sound power level used in this study is determined in decibel (dB) according to [1]:

$$L_w = \overline{L_p} + 10\,lg\frac{A_D}{A_0} - 10\,lg\frac{\rho c}{(\rho c)_0}, \quad (5)$$

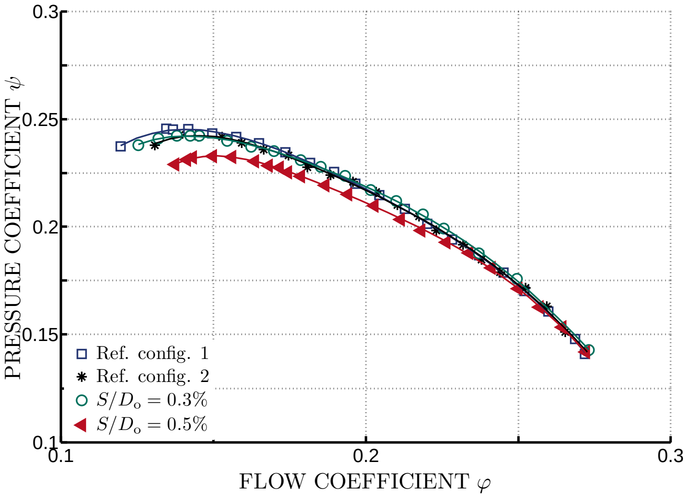

FIGURE 4. INFLUENCE OF THE PERFORATED CASING ON THE PRESSURE COEFFICIENT

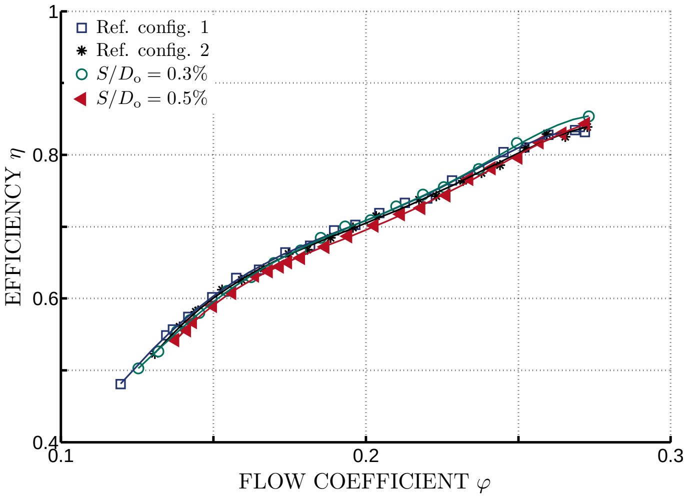

FIGURE 5. INFLUENCE OF THE PERFORATED CASING ON EFFICIENCY

where $A_0 = 1\ \mathrm{m}^2$ is a reference cross sectional area and $(\rho c)_0 = 400\ \mathrm{Ns/m}^3$ is the acoustic impedance at standard conditions. $\overline{L_\mathrm{p}}$ is the corrected sound pressure level determined according to [1]. In order to be able to compare fans with different size and power, Madison [6] introduced the specific sound power

$$L_\mathrm{wspez} = L_\mathrm{w} - 10\, lg \frac{\dot{V}}{\dot{V}_0} - 20\, lg \frac{\Delta p_\mathrm{t}}{\Delta p_0}, \tag{6}$$

which will be used in this study.

RESULTS

To determine the aerodynamic and acoustic characteristics 22 operating points in average are measured and evaluated for every configuration [7]. All points shown in this study are measured with the measurement technique described above, while the lines are interpolated with a 5th degree polynomial, with exception of Fig. 10 and plots of the frequency spectra.

Influence of the Perforated Casing

In the blade tip region of a turbomachine, the structure of the casing wall plays an important role in development of tip clearance flow and resulting tip leakage vortices. In reference to applications in aviation, several studies regarding the effect of casing treatments and structures have been performed. With the measurements in this study, no statements about fluid mechanics and interaction between flow and casing can be made. Rather the influence on total pressure rise, efficiency and emitted sound power level is determined with the help of two reference measurements. As shown in Fig. 3 for the first reference configuration, the backside of the perforated surface is sealed with an airtight thin adhesive foil and a sound-reflecting steel plate. To determine the influence of the perforation, a second reference configuration with a plain casing and the same tip clearance is necessary. Therefore, the perforation was sealed with paraffin to receive a plain surface. In Fig. 4, the influence of the perforated casing on the aerodynamic characteristics of the fan in comparison with a hardwall plain casing, as shown in Fig. 2 with relative tip clearances $s = S/D_\mathrm{o} = 0.3\%$ and $s = 0.5\%$ is shown by pressure coefficient ψ versus flow coefficient φ. Influence of the tip clearance, mainly in the range of lower flow coefficients, can be seen regarding the difference between the curves of $s = 0.3\%$ and $s = 0.5\%$. It is noticeable that reference configuration 1 shows a slightly higher pressure coefficient and a larger operating range than reference configuration 2 with a plain surface. Apparently the perforated surface works as a casing treatment, in case it has a positive interaction with the casing boundary layer and a positive influence on the near casing flow. Figure 5 shows the influence on efficiency. With exception of the curve with a relative tip clearance of $s = 0.5\%$, differences are in the limits of uncertainty of measurement. Figures 4 and 5 point out that the perforated surface has a slightly positive effect on the aerodynamic characteristics of this fan. Regarding the acoustic characteristics in Fig. 6, the influence of tip clearance can clearly be recognized between the curves of the relative tip clearances $s = 0.3\%$ and $s = 0.5\%$, especially in range of lower flow coefficients. The perforated surface of the casing ring shows a positive influence on sound emission of the fan. Taking the reference configuration with the plain surface as a basis, Fig. 7 plots differences in specific sound power versus the flow coefficient. It can be seen that the emitted specific sound power of the reference configuration with the perforated surface is lower than the configuration

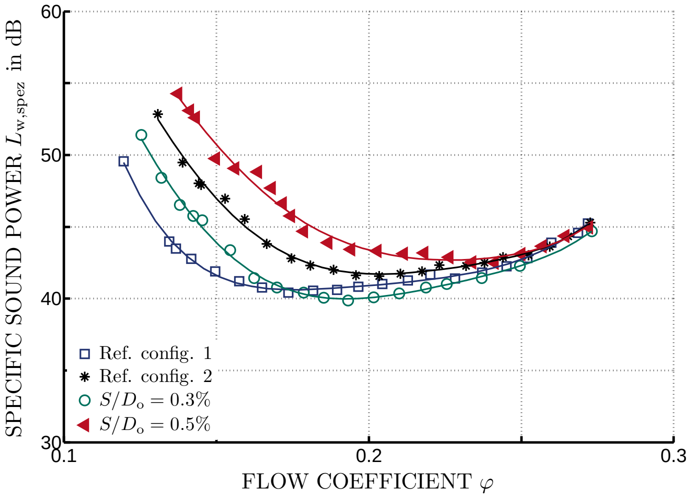

FIGURE 6. INFLUENCE OF THE PERFORATED CASING ON THE SPECIFIC SOUND POWER

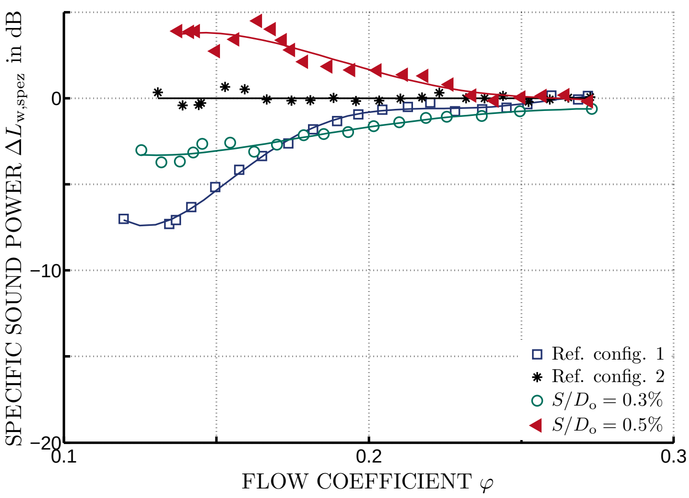

FIGURE 7. INFLUENCE OF THE PERFORATED CASING ON THE SPECIFIC SOUND POWER

with the plain surface for the whole operating range. At the design point of the used fan configuration $\varphi = 0.17$, the reduction is $\Delta L_{w,spez} \approx 2.9$ dB. Maximum difference occurs in the range of lower flow coefficients and hence, maximum influence of tip clearance noise and is $\Delta L_{w,spez} \approx 7.1$ dB.

In Fig. 8, the frequency spectra over the complete operating range are shown for the two reference cases and with absorber material HR290/71. Remarkable are the peaks at 41.66 Hz and 375 Hz, which correspond to the rotational speed and the blade passing frequency (BPF). The plot for reference configuration 2 shows the development of tip clearance noise for lower flow co-

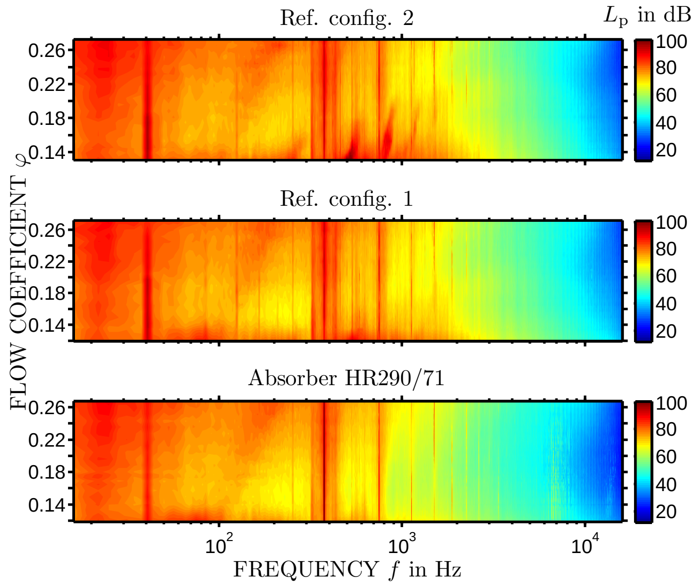

FIGURE 8. INFLUENCE OF THE PERFORATED CASINGON THESOUND SPECTRA FOR COMPLETE OPERATING RANGE

efficients and the frequency shift of these peaks towards lower frequencies for decreasing flow coefficients. This was also found by [2]. In the frequency spectra for reference configuration 1, a reduction of the tonal frequencies between the BPF and the first, second and third harmonic can be seen. The influence of the absorber material shows a broadband reduction of the sound level, which will be analyzed in a second step. Figure 9 shows the frequency spectra, pointing out the influence of the tip clearance. The increase of specific sound power can be traced back mainly to a discrete raise of the peaks between the BPF and its first two harmonics.

Absorption Coefficients of the Used Materials

To determine the acoustic characteristics, the absorption coefficients of the studied absorber materials are measured using an impedance tube, also known as Kundt's tube. With the experimental setup according to [8], the reflection and absorbing characteristics at a normal sound incidence of a sample can be measured. Since only stationary waves can be measured reproducibly, only frequencies below the first cut-on frequency f_{cut-on} are measured. For the given inner diameter of the impedance tube of 107 mm and a speed of sound $c = 340$ m/s for air at standard conditions, the limiting frequency is $f_{cut-on} = 1862$ Hz. Figure 10 shows results of the measurements, the absorption coefficient α versus the frequency f. The absorption coefficient rises with increasing frequency of the stationary wave in the tube. Efficiency of an absorber depends on its location in reference to the sound particle velocity spectrum, because absorption is subject to

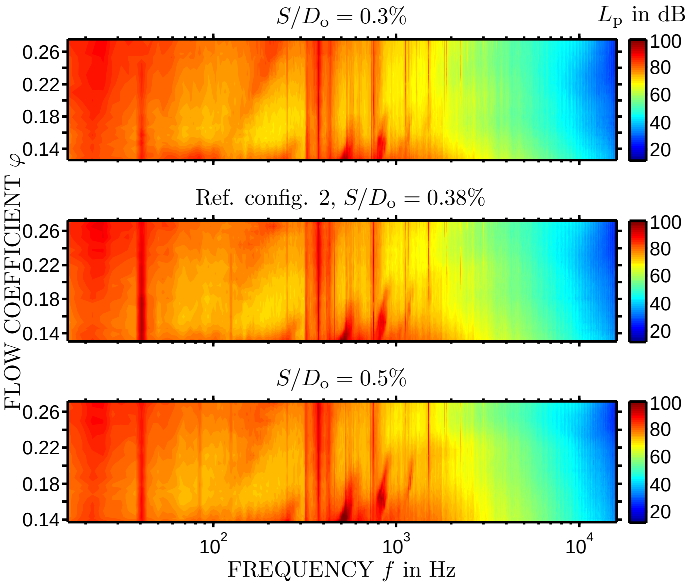

FIGURE 9. INFLUENCE OF THE TIP CLEARANCE ON THE SOUND SPECTRA FOR COMPLETE OPERATING RANGE

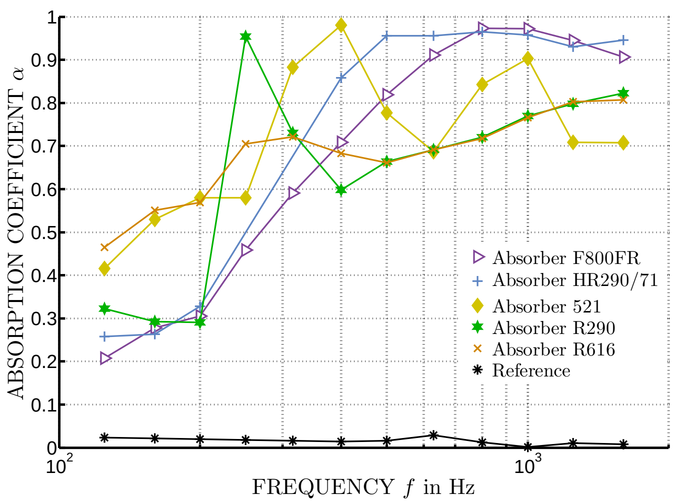

FIGURE 10. ABSORPTION COEFFICIENT OF THE USED MATERIALS WITH A THICKNESS OF 100 mm

the kinetic energy of the particles in the absorber. On the surface of the sound-reflecting termination, the sound particle velocity approaches zero, hence it approaches its maximum at $\lambda/4$. If the wavelength of the stationary wave increases with regard to absorber thickness and the maximum sound particle velocity at $\lambda/4$ is not located inside the absorber, the absorption coefficient decreases. In theory the peak absorption coefficient is obtained when the maximum sound particle velocity reaches the surface

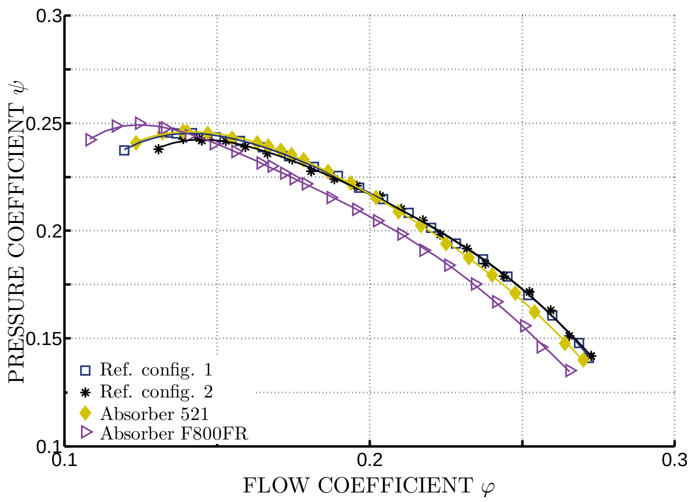

FIGURE 11. AERODYNAMIC CHARACTERISTICS FOR CONFIGURATIONS WITH SOUND ABSORBERS

of the absorber material. The frequency of the first maximum changes with the characteristics of the material, due to a change in velocity of propagation and hence, wave length, during the transition into the absorber material. In the present case, considering the same thickness of all tested materials (100 mm), macroscopic viscous and thermal behaviour as well as elastic properties of each porous material cause different absorbing characteristics. In [9] it was shown by Möser that next to the velocity of propagation c_a the structure factor χ of the material also has an influence on the frequency of the first maximum. For higher frequencies a decrease in α is found because the absorber is not exploited optimally any more, which is shown by the wave characteristic of the curves in Fig. 10 for larger frequencies. Regarding the measurements of the absorber materials, F800FR and HR290/71 show the best results over the measured frequency range. The measured reference in Fig. 10 is equal to reference configuration 2 with the plain surface studied in the fan test rig. In this case, no absorber material was installed in front of the sound-reflecting termination. All absorber materials were also measured behind a perforated plate to study the influence of the perforated casing. Within the uncertainty in measurement, no considerable influence could be found.

Measurements with Sound Absorber

Measurements of two reference cases in the fan test rig show the influence of the perforated casing while the characteristics of the used absorber materials are tested in the impedance tube. The results of the measurement with the complete setup as shown in Fig. 3 on the right side with five different absorber materials behind the perforated ring under aerodynamic and acoustic aspects are shown in this section. Figures 11 and 12 show the aero-

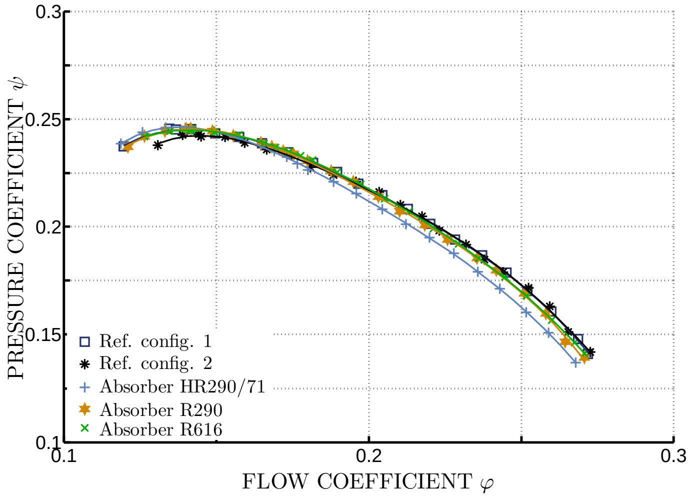

FIGURE 12. AERODYNAMIC CHARACTERISTICS FOR CONFIGURATIONS WITH SOUND ABSORBERS

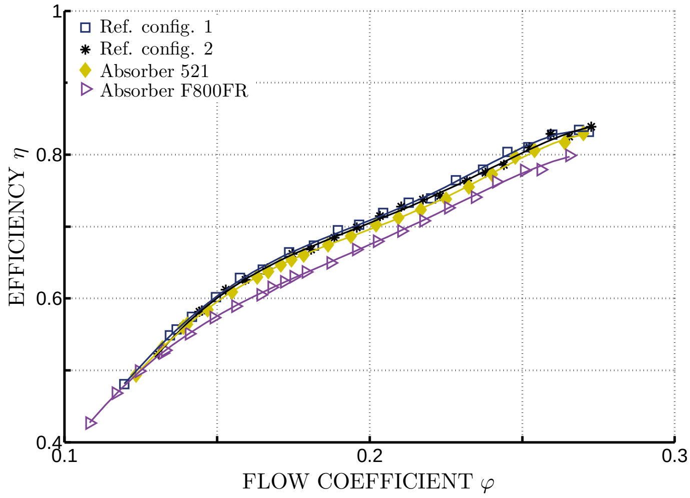

FIGURE 13. EFFICIENCY FOR CONFIGURATIONS WITH SOUND ABSORBERS

dynamic characteristics of the configuration with five absorber materials. For reference purposes, the configurations with plain and perforated surfaces are additionally plotted. To determine the influence of the absorber material, the difference to reference configuration 1 has to be considered. The installation of the materials 521, R290 or R616 does not cause a significant change in total pressure rise, and only a slight descent at higher flow coefficients can be found. For the materials HR290/71 and F800FR, which subjectively[1] have a lower flow resistance than the other materials, this trend is clearly stronger. Nearly over the complete stable operating range, a significant decrease of the pressure coefficient is found, whereas for very small flow coefficients, the two absorber materials show a higher total pressure rise and even an enlargement of the operating range. Because of the low flow resistance of these materials, air is able to stream into the absorber materials. Due to the pressure difference between the stage in- and outlet on the one hand, and the pressure and the suction side in the near casing area of the blades on the other hand, the flow recirculates through the absorber. This leakage flow does not participate in energy transformation of the fan, and the flow through the absorber causes additional losses. Also remarkable is the shift of the maximum flow coefficient towards lower values for the point measured with the throttle completely open, for the materials HR290/71 and F800FR. This can also be traced back to recirculation of the flow through the absorber material. This flow is driven by the fan, but it is not recognized by the inlet nozzle. It suggests itself, that the whole characteristic is shifted towards smaller flow coefficients.

Efficiencies of the studied absorbers in Fig.13 and Fig.14 show the same trend. The efficiency η of the materials 521, R290 and R616 is about $\Delta\eta \approx 1-1.5\%$ lower than the reference case with the perforated surface. For absorber material HR290/71, the influence is $\Delta\eta \approx 2.5\%$, and for F800FR even $\Delta\eta \approx 3-3.7\%$.

The influence of the used absorber materials on the acoustic characteristics of the fan are shown in Fig. 15 and Fig. 16. As a basis, the reference configuration with the plain surface is used again. Absorber material R290 shows a good effectiveness over the complete operating range. Especially for small flow coefficients at $\varphi \approx 0.13$, this configuration can reduce the emitted sound power about $\Delta L_{\mathrm{w,spez}} \approx 10.6$ dB, whereby 7.1 dB result

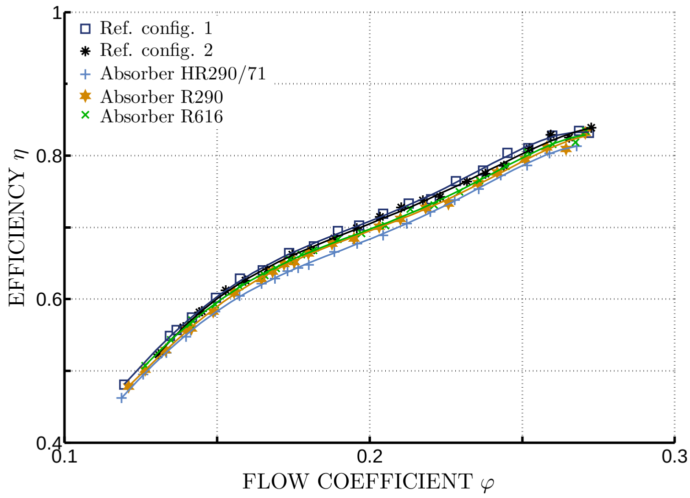

FIGURE 14. EFFICIENCY FOR CONFIGURATIONS WITH SOUND ABSORBERS

[1]No measurements regarding an exact value of flow resistance of the materials have been performed, therefore only a subjective assessment can be given.

from the perforated casing as shown earlier in Fig. 7. In the design point of this fan configuration $\varphi = 0.17$, the specific sound power could be reduced by $\Delta L_{\mathrm{w,spez}} \approx 4$ dB, 2.9 dB result from the perforated casing. For larger flow coefficients, the influence of the sound absorber decreases. This is due to the tip clearance noise not being as dominant in this operating range. The results of the measurements in the impedance tube show that material R290, regardless of the first maximum at $f \approx 250$ Hz, does not reach absorption coefficients of $\alpha \geq 0.8$ until $f \geq 1250$ Hz. In Fig. 17, the frequency spectrum and the third octave band for a flow coefficient $\varphi = 0.17$ is shown for the two reference cases and absorber material R290. In the frequency spectrum, the influence of the absorber material can be recognized for frequencies higher than the second harmonic ($f \geq 1125$ Hz). The tonal frequencies between the BPF and the first, second and third harmonic, which already have been nearly completely reduced by the perforated surface, do not appear for the configuration with R290 either. The second recycling material, R616, shows a similar behavior as R290, although the effect of the sound absorber for high flow coefficients decreases. For the design point $\varphi = 0.17$, the reduction of the specific sound power is $\Delta L_{\mathrm{w,spez}} \approx 3.6$ dB and close to the stall region $\varphi = 0.13$ even $\Delta L_{\mathrm{w,spez}} \approx 9.9$ dB. The acoustic measurements in the test rig with absorber material HR290/71, which has good absorption coefficients during the experiments in the impedance tube, show that the sound absorption in the fan test rig is not nearly as good. Over almost the whole operating range, the emitted sound power is higher than for the reference case with the perforated surface, for large flow coefficients even higher than for the plain surface. The frequency spectrum in Fig. 18 shows that in accordance to the results of the measurements in the impedance tube, a broadband absorption takes effect from $f \approx 300$ Hz. The comparison with R290 shows that for $f \geq 3000$ Hz, both materials show nearly the same sound power level, but below that value HR290/71 has significant better absorption characteristics. A precise analysis of all recorded data also shows that, as found in the impedance tube, HR290/71 has the best absorbing characteristics. The strong raising of the BPF in Fig. 18 also gives the explanation for the higher specific sound power level. At the operating point ($\varphi \approx 0.15$), the sound level of the BPF is more than 13 dB higher than for the reference case and rises by 15.4 dB for $\varphi \approx 0.13$. A possible explanation is the configuration of the absorber materials, which have to be parted due to the flange on both sides of the casing ring. Additionally, the surface of HR290/71 has a grooved structure. The grooves and tiny gaps between parts of absorber materials could be responsible for the raise of the BPF.

Absorber material F800FR reduces the specific sound power level over most of the operating range (Fig. 19). For $\varphi = 0.17$, the advantage over the perforated casing is 0.4 dB. For part load, the effect of the absorber material increases. But keeping in mind the efficiency loss, this result does not justify the effort in terms of material and space used. Similar to HR290/71 and according

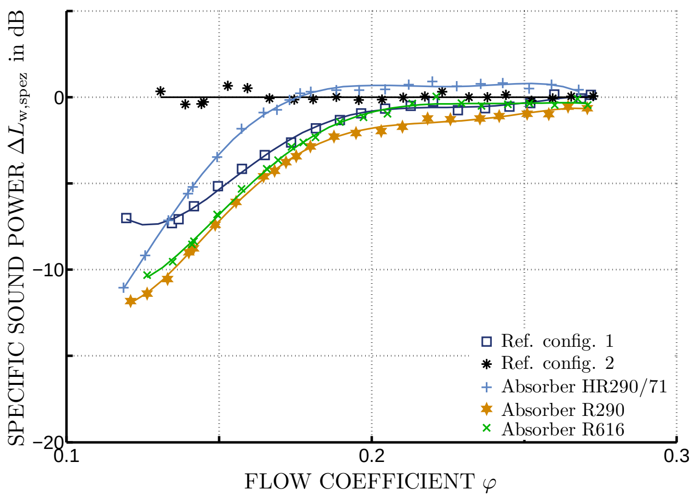

FIGURE 15. DIFFERENCE IN SPECIFIC SOUND POWER FOR CONFIGURATIONS WITH SOUND ABSORBERS

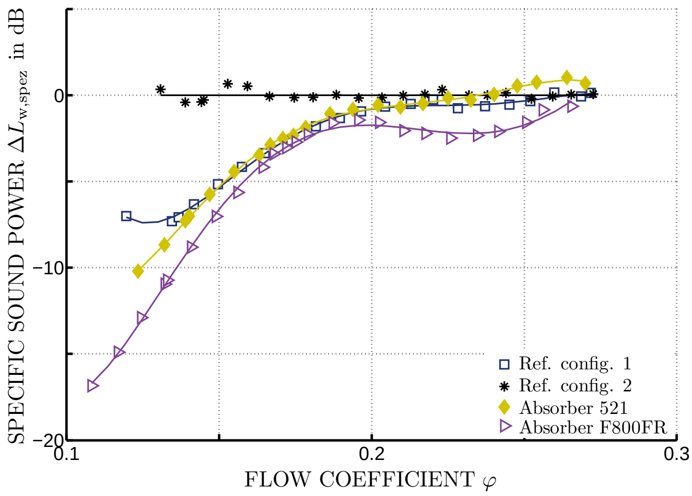

FIGURE 16. DIFFERENCE IN SPECIFIC SOUND POWER FOR CONFIGURATIONS WITH SOUND ABSORBERS

to measurements in the impedance tube, this absorber material takes effect from $f \approx 300$ Hz (Fig. 19). Because of its increase the third harmonic becomes the dominant frequency in this case and prevents better results in the specific sound power level. The last studied absorber material, 521, shows no significant difference to reference case 1 with the perforated casing. Analysis of the frequency spectrum again shows that the positive effect of the absorber especially for frequencies $f > 800$ Hz is compensated by an increase of the BPF.

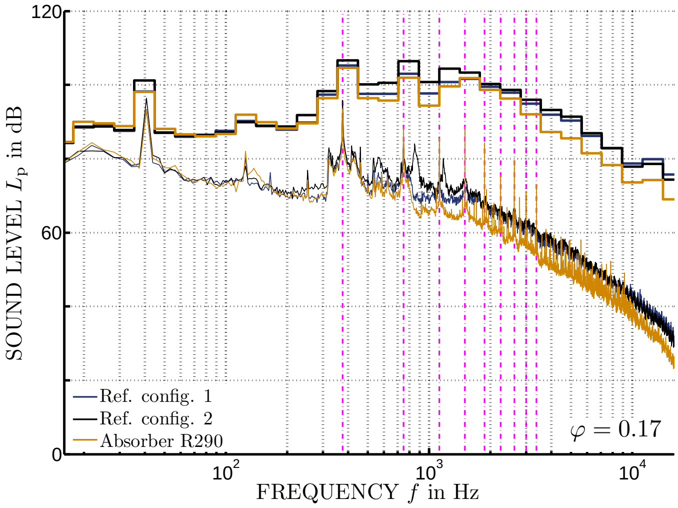

FIGURE 17. FREQUENCY SPECTRUM FOR CONFIGURATIONS WITH SOUND ABSORBER R290

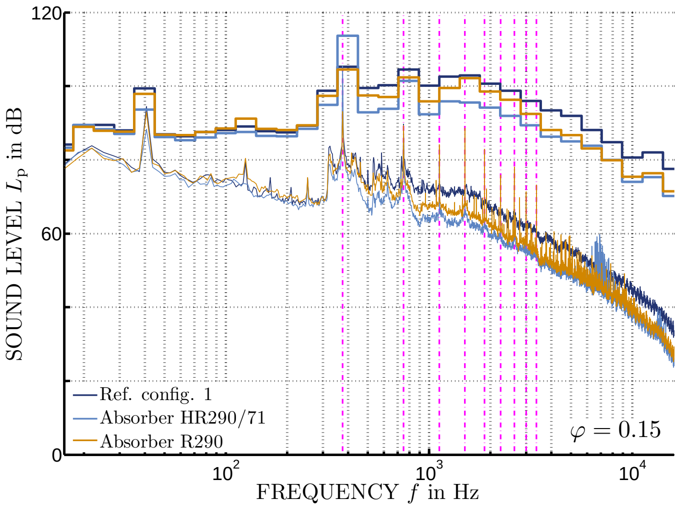

FIGURE 18. FREQUENCY SPECTRUM FOR CONFIGURATIONS WITH SOUND ABSORBER HR290/71 AND R290

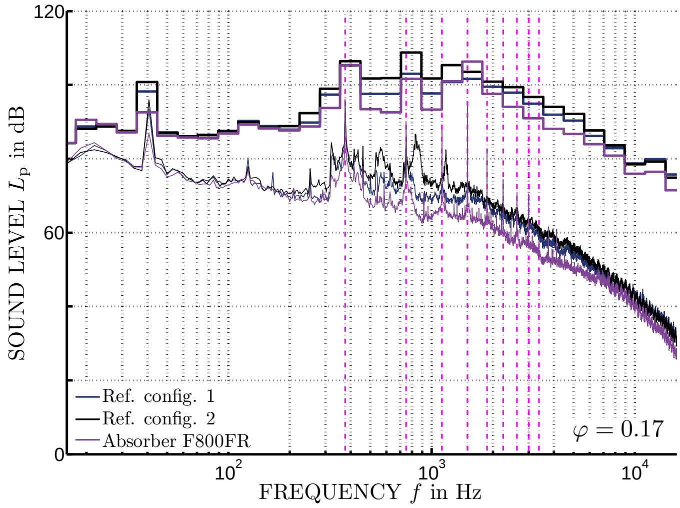

FIGURE 19. FREQUENCY SPECTRUM FOR CONFIGURATIONS WITH SOUND ABSORBER F800FR

CONCLUSION

The present study deals with the efficiency of an absorber configuration installed in the rotor region of a fan with nine skewed blades. The absorber is an assembly of a perforated casing ring with an installed absorber and a sound-reflecting termination. The effect of the perforated surface on the aerodynamic and acoustic characteristics of the fan is determined with two reference measurements. The acoustic characteristics of the used materials are measured in an impedance tube to gain information about the absorption coefficient and its frequency dependence. The studies in the fan test rig show that the positive results of the absorber configurations are a combination of two effects. Through the influence of the perforated casing structure in the region of the fan rotor, a significant reduction of the emitted sound power can be achieved. This is caused by an reduction of the tonal peaks between the BPF and its first three harmonics. Because these peaks increase with a decreasing flow coefficient, the efficiency of the perforated casing also increases for this operating range. Through the installation of absorber materials, the mentioned peaks are further reduced, which increases the effect of the absorber for smaller flow coefficients. The second positive effect is the noise reduction of the sound absorber, which causes a broadband reduction of the sound level, especially for higher frequencies. Dimension and frequency of the sound absorbing effect depend significantly on the operating point and used absorber material. Deviant from the mentioned positive effects, the installation of absorber materials in some configurations causes a significant increase of tonal frequencies, which reduces or even prevents the effect of global absorption.

REFERENCES

[1] ISO 5136, 2003. *Acoustics - Determination of sound power radiated into a duct by fans and other air-moving devices - In-duct method*. Berlin, Beuth Verlag.

[2] Karstadt, S., Heß, M., Matyschok, B., and Pelz, P. F., 2010. "The influence of tip clearance on the acoustic and aerodynamic characteristics of fans". *Proceedings of ASME Turbo Expo 2010, GT2010-22082*.

[3] Fukano, T., and Jang, C.-M., 2004. "Tip clearance noise of axial flow fans operating at design and off-design condition".

Journal of Sound and Vibration (2004), Vol.275.

[4] Emmrich, R., Höhnen, H., and Niehuis, R., 2009. "Time resolved experimental investigations of an axial compressor with casing treatment". *Journal of Turbomachinery (2009), Vol. 131*.

[5] Hathaway, M., 2002. "Self-recirculating casing treatment concept for enhanced compressor performance". *Proceedings of ASME Turbo Expo 2002, GT-2002-30368*.

[6] Madison, R., 1949. *Fan Engineering (Handbook) 5th ed.* Buffalo Forge, Buffalo, New York.

[7] Croll, J., 2008. "Schalldämmung am Ventilator". Diploma thesis, Technische Universität Darmstadt.

[8] ISO 10534, 2001. *Acoustics Determination of sound absorption coefficient and impedance in impedance tubes*. Berlin, Beuth Verlag.

[9] Möser, M., 2005. *Technische Akustik 6th ed.* Springer Verlag, Berlin.

